

Pattern formation and instability of flow between two corotating disks

Tomohito Miura and Jiro Mizushima*

Department of Mechanical Engineering, Faculty of Engineering, Doshisha University,
Kyotanabe, Kyoto 610-0321, Japan

E-mail: jmizushi@mail.doshisha.ac.jp*

Abstract. Transition of flow between two corotating disks in an enclosure is investigated numerically and experimentally, in which the origin of polygonal flow pattern is explored utilizing numerical simulation, bifurcation analyses of the numerical data and the linear stability theory. The outer cylindrical boundary of the flow field is assumed to be stationary, whereas the inner cylinder rotates together with the two disks. Polygonal flow patterns are known to appear due to instability of the axisymmetric flow around the axis of rotation, which is a unique solution at small Reynolds numbers. The origin of the flow structure of so called shift-and-reflect flow pattern is clarified from the solution of the linear stability analyses. In addition, we found that the most unstable mode of disturbance has an unexpected wavenumber as large as 20 to 30 for very narrow disk spacings.

1. Introduction

Flow between two corotating disks in a fixed cylindrical enclosure has been investigated in engineering applications such as turbomachinery, chemical reactor and so on though it attracts theoretical interest. If the inter-disk spacing is very small compared with the radius of the disks, the flow is regarded as a simplified model of flow in computer disk storages. It is well known that the flow field loses a symmetry around rotation axis and displays the complexity when the two disks rotate at large angular velocity.

For the purpose to reduce flutters in computer disk storages, Lennemann[1] examined the structure of non-axisymmetric flow field using visualization technique in detail, and reported that polygonal shaped flow patterns appear in the horizontal plane and the pattern rotates at about 80% of the disk rotation rate. The polygonal flow patterns appeared as a first bifurcation of axisymmetric flow when the ratio of the inter-disk spacing to the width of the annulus, say the length ratio L , was less than about 0.3.

The formation of the polygonal flow field was investigated by Abrahamson, Eaton and Koga[2], who performed flow visualization of the flow for small length ratios and identified three distinct regions in the polygonal flow field, i.e. an inner and outer regions and a shroud boundary layer. The inner region is characterized by rigid-body rotation near the inner cylinder and the outer region is occupied by large vortices. The inner and outer regions are separated by a polygonal shape of boundary. There are many small vortices in the shroud boundary layer. It is also reported that the number of structures decreases in a stepwise manner as the rotation speed of disks increases.

Schuler, Usry, Weber, Humphrey and Greif[3] measured the mean and root mean square (rms) azimuthal velocity component of the flow between two corotating disks by using Laser-Doppler Velocimeter (LDV). Their measurements revealed that the flow near the inner cylinder is in rigid-body rotation and a strongly sheared flow is present near the outer cylinder. Also, their theoretical analyses suggested that the flow structure changes from two-dimensional to three-dimensional in the detached shear layer located between the inner and outer regions. The breaking of the axisymmetry was investigated in experiment by Humphrey and Gor[4], who evaluated the location and thickness of the detached shear layer. They showed that the detached shear layer and the outer region oscillate above a critical Reynolds number, and a circumferentially-periodic flow structure appears in the horizontal plane. Humphrey, Shuler and Webster[5] carried out numerical simulation to reveal the three-dimensional structure of the flow field for the configuration that was considered by Shuler *et al.*[3]. Their numerical results showed qualitative agreement with the experimental results by Humphrey and Gor[4]. They found that the number of vortices observed in the horizontal plane is an even integer. This is because the wavelength of azimuthal velocity component is twice that for an axial velocity component. However, their results did not show quantitative agreement with the experimental measurements obtained by Shuler *et al.*[3]. Recently, Herrero and Humphrey and Giralt[6] reported that the difference between numerical and experimental results is avoidable if they consider the presence of radial clearances or gaps between the rims of the disks and the outer cylinder, and the finite thickness of the disks in numerical calculation.

Transitions of the flow were investigated by Herrero, Giralt and Humphrey[7], who considered the effect of the length ratio on the transition by numerical simulation and revealed that an axisymmetric steady flow bifurcates into two different families of unsteady three-dimensional flow. For large length ratios, the bifurcated flow field is asymmetric with respect to inter-disk midplane, while the flow field displays a shift-and-reflect symmetry with respect to inter-disk midplane for small length ratios. Hirata, Furue, Sugawara and Funaki[8] confirmed these different structures of the flow field experimentally using three-dimensional PIV (Particle Image Velocimetry) methods. The transition of the flow was investigated also by Randriamampianina, Schiestel and Wilson[9] and a regime diagram of the bifurcation was obtained in a parameter space consisting of the Reynolds number and the length ratio. From the diagram, a critical length ratio is determined as $\Gamma_c \sim 0.26$, below which the fluid motion becomes time-dependent before bifurcating to a steady asymmetric flow. For $\Gamma > \Gamma_c$, an unsteady three-dimensional flow occurs after the transition to a steady asymmetric flow, and the structure of the flow displays a shift-and-reflect symmetry. They found that multiple solutions develop with the presence of quasi-periodic behaviour resulting from successive vortex pairings.

In the present paper, we investigate the flow structure of the flow between two corotating disks in detail by numerical calculation, linear stability analysis and flow visualization, and clarify the bifurcation structure of the flow in the range of the length ratios $0.2 \leq \Gamma \leq 0.6$. Our major objective is to explore the origin of the polygonal flow patterns.

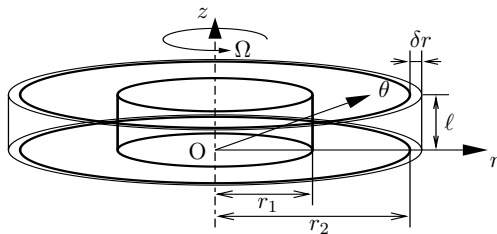


Figure 1. Configuration and coordinates.

2. Formulation of problem

We consider fluid motions between two corotating disks in an enclosure as illustrated in Fig. 1. The outer cylinder of radius r_2 is stationary, while the inner cylinder of radius r_1 rotates together with the two disks at angular velocity Ω . The gap δr between the edge of disks and the outer cylinder is very narrow and neglected in the present paper. Taking $r_2\Omega$ and d ($\equiv r_2 - r_1$) as characteristic velocity and length scales, we define the Reynolds number Re as $Re \equiv r_2\Omega d/\nu$, where ν is the coefficient of kinematic viscosity of the fluid. The spacing between the two disks, i.e. the length of the cylinders, is ℓ and the length ratio Γ is defined by $\Gamma \equiv \ell/d$. Various flow patterns appear depending on a set of parameters (Γ, Re) . There is another nondimensional parameter, the radius ratio $\eta = r_1/r_2$, which is assumed to be 0.5 throughout this paper.

We take the cylindrical coordinates $\mathbf{r} = (r, \theta, z)$ as shown in Fig. 1 and denotes the velocity and the pressure as $\mathbf{u} = (u, v, w)$ and p , respectively. Then, the dimensionless continuity and momentum equations for u, v, w and p are written as

$$\frac{1}{\xi_\beta} \frac{\partial(\xi_\beta u)}{\partial \xi} + \frac{1}{\xi_\beta} \frac{\partial v}{\partial \theta} + \frac{\partial w}{\partial z} = 0, \quad (1)$$

$$\frac{\partial u}{\partial t} + u \frac{\partial u}{\partial \xi} + \frac{v}{\xi_\beta} \frac{\partial u}{\partial \theta} + w \frac{\partial u}{\partial z} - \frac{v^2}{\xi_\beta} = -\frac{\partial p}{\partial \xi} + \frac{1}{Re} (\nabla^2 u - \frac{u}{\xi_\beta^2} - \frac{2}{\xi_\beta^2} \frac{\partial v}{\partial \theta}), \quad (2)$$

$$\frac{\partial v}{\partial t} + u \frac{\partial v}{\partial \xi} + \frac{v}{\xi_\beta} \frac{\partial v}{\partial \theta} + w \frac{\partial v}{\partial z} + \frac{uv}{\xi_\beta} = -\frac{1}{\xi_\beta} \frac{\partial p}{\partial \theta} + \frac{1}{Re} (\nabla^2 v - \frac{v}{\xi_\beta^2} + \frac{2}{\xi_\beta^2} \frac{\partial u}{\partial \theta}), \quad (3)$$

$$\frac{\partial w}{\partial t} + u \frac{\partial w}{\partial \xi} + \frac{v}{\xi_\beta} \frac{\partial w}{\partial \theta} + w \frac{\partial w}{\partial z} = -\frac{\partial p}{\partial z} + \frac{1}{Re} \nabla^2 w, \quad (4)$$

where

$$\xi = r - \frac{r_1}{d}, \quad \xi_\beta = \xi + \frac{r_1}{d} \quad \text{and} \quad \nabla^2 = \frac{\partial^2}{\partial \xi^2} + \frac{1}{\xi_\beta} \frac{\partial}{\partial \xi} + \frac{1}{\xi_\beta^2} \frac{\partial^2}{\partial \theta^2} + \frac{\partial^2}{\partial z^2}.$$

The non-slip boundary conditions for u, v and w are given as

$$u = w = 0, \quad v = \eta \quad (5)$$

at the inner cylindrical surface ($\xi = 0$) and the conditions

$$u = w = 0, \quad v = 0 \quad (6)$$

are applied on the fixed enclosure wall ($\xi = 1$). Since we assume that the two disks rotate together with the inner cylinder, the boundary conditions at the top and bottom boundaries ($z = 0, \Gamma$) are written as

$$u = w = 0, \quad v = \eta + \xi(1 - \eta). \quad (7)$$

Dynamical equations (2) – (4) constitute the basic equations together with continuity equation (1), which are solved numerically under the appropriate boundary conditions as an initial value problem.

The flow between two corotating disks in a fixed enclosure is steady and axisymmetric at small Reynolds numbers irrespectively of the value of the length ratio. However, the steady axisymmetric flow becomes unstable to disturbances to exhibit polygonal flow patterns. In order to explore the origin of the appearance of polygonal flow patterns in the instability of the steady axisymmetric flow (basic flow), we investigate the linear stability of the basic flow with respect to non-axisymmetric disturbances.

The basic flow $(\bar{\mathbf{u}}, \bar{p})$ satisfies steady-state equations which are obtained dropping the term with a time derivative in dynamical equations (2) – (4) as well as the continuity equation (1).

For the linear stability analysis of the basic flow, we suppose an infinitesimal non-axisymmetric disturbance (\mathbf{u}', p') added to the basic flow and express the velocity and the pressure as $\bar{\mathbf{u}} + \mathbf{u}'$ and $\bar{p} + p'$, respectively. Considering the spatial periodicity, the disturbance is decomposed into a Fourier series in the azimuthal variable θ , of which only one component (mode) is considered separately because of the linearity of the disturbance and expressed as:

$$\mathbf{u}' = \tilde{\mathbf{u}}_k e^{ik\theta}, \quad p' = \tilde{p}_k e^{ik\theta}, \quad (8)$$

where k is a wavenumber in the azimuthal direction. Substituting these expressions into Eqs. (1) – (4), subtracting the equations for the basic flow and neglecting the nonlinear terms of the disturbance, we obtain linearized time dependent equations for the disturbance. The boundary conditions for the disturbance are given as

$$\mathbf{u}' = 0 \quad (9)$$

on all rigid boundaries. Each Fourier mode of the disturbance is solved numerically as an initial value problem. The stability of the basic flow with respect to the disturbance with a Fourier mode k is determined by evaluating the linear growth rate of the disturbance energy E_k , in which the energy is expected to vary exponentially with time after sufficiently long time elapsed as

$$E'_k = E'_{k0} \exp(\lambda_k t), \quad (10)$$

where λ_k is the linear growth (or decay) rate of the disturbance with the Fourier mode k . The basic flow is stable to the mode of disturbance, if $\lambda_k < 0$, or unstable if $\lambda_k > 0$.

3. Numerical and experimental methods

Three-dimensional numerical simulation is performed to obtain polygonal flows, in which the HSMAC (Highly Simplified MAC) method is utilized on a staggered uniform grid. The derivatives in the convection terms are approximated using a third-order-accuracy upstream difference, and a fourth-order-accuracy central finite difference approximation is used in the diffusion term. We adopt the Adams-Bashforth scheme with second-order-accuracy for the time integration. The periodic boundary condition is imposed in the the azimuthal direction. For numerical calculation in the linear stability analysis, a fractional step method is used and the convection, diffusion and time differentiation terms are discretized in the same way with those in numerical simulation. The pressure equation is approximated by a second-order-accuracy central difference and is solved using SOR (Successive Over Relaxation) method.

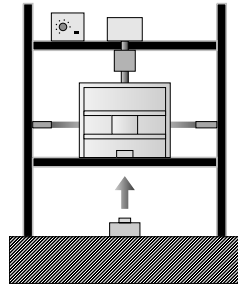


Figure 2. Experimental apparatus.

Pictures of polygonal flow pattern are taken by flow visualization in experiment, where water ($\nu = 1.61 \times e^{-0.0228t}$, t : water temperature) is used for the working fluid and the flow field is

visualized by Aluminium powder. A sheet of light is thrown horizontally to the fluid layer at its mid height and the flow pattern in the horizontal plane is taken by a digital video camera. The experimental apparatus we used is shown in Fig. 2. Two rotational disks of radius 197 ± 0.5 mm, the outer cylinder of radius 200 ± 0.5 mm and the inner cylinder of radius 30 ± 0.025 mm are made of transparent acrylic resin for visualization. The gap between the two disks is varied in the range of 10 mm – 30 mm.

4. Results and discussion

4.1. Numerical simulation

We adopted $\Gamma = 0.6$ as a typical length ratio to investigate the transition of the flow in our numerical simulation, in which the Reynolds number is taken in the range $750 \leq Re \leq 1000$ and the number of grid point is taken as $80 \times 60 \times 60$. An example of the flow pattern is shown in Fig. 3 for $Re = 750$, where solid and dashed lines indicate positive and negative value of the stream function, respectively. A pair of vortical structure, which is symmetric with respect to the inter-disk midplane, is recognized near the fixed enclosure. It is observed in Fig. 3 that the flow field is steady and symmetric with keeping the axisymmetry. For a larger Reynolds number as $Re = 1000$, numerical simulation was carried by using the solution obtained at $Re = 750$ as an initial condition. After long time integration, the flow field lost the axisymmetry and a flow pattern having a wavy structure in the azimuthal direction appeared. Figure 4 shows contours of velocity components (u, v, w) and axial vorticity ω_z in the horizontal plane in the flow field at $Re = 1000$. Each velocity component exhibits an azimuthal mode with wavenumber $k = 3$. As shown in Fig. 4(d), three large vortices occupy almost the whole flow field and form a shape of triangle in the flow field.

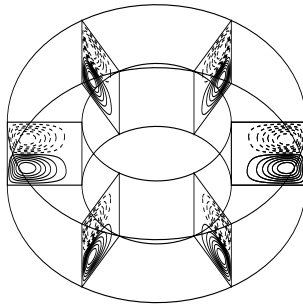


Figure 3. Flow pattern (stream lines) at different meridional planes. $\Gamma = 0.6$. $Re = 750$. Solid line: positive value of the stream function. Dashed line: negative value of the stream function.

In order to evaluate the growth rate of the mode of disturbance with the wavenumber k , we define the kinematic energy of the mode by

$$E_k = \int \int \int \mathbf{u}_k \cdot \bar{\mathbf{u}}_k r dr d\theta dz, \quad (11)$$

where \mathbf{u}_k is the velocity component with the wavenumber k , and examine the magnitude of E_k in the equilibrium state in the range of $750 \leq Re \leq 1000$. The value of E_3 is depicted as a function of Re in Fig. 5, from which we see that E_3 grows above a critical Reynolds number $Re_{c1} = 817$, i.e. the steady axisymmetric flow becomes unstable at Re_{c1} and a polygonal flow pattern with wavenumber $k = 3$ appears above the critical value.

Figure 6 shows instantaneous flow patterns at different meridional planes sectioned in every half azimuthal wavelength at $Re = 1000$ for $\Gamma = 0.6$, where solid and dashed lines indicate negative and positive values of the stream function, respectively. In the section of $\theta = 0$

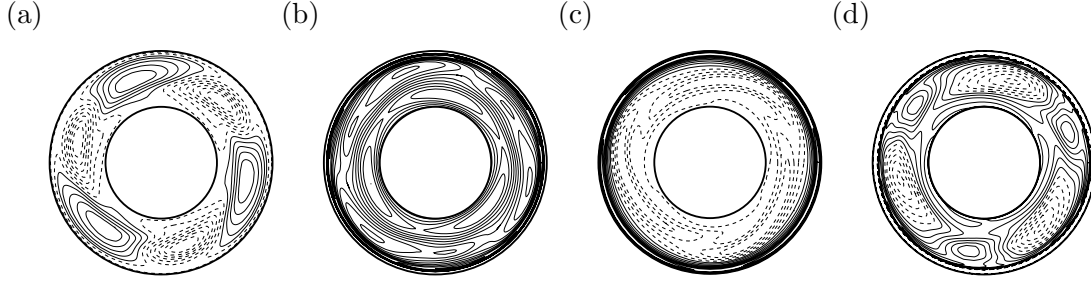


Figure 4. Flow pattern in the horizontal plane. $\Gamma = 0.6$. $Re = 1000$. $z = 0.25 \Gamma$. Solid and dashed lines indicate positive and negative value of each physical quantity. (a) Contour lines of u , (b) v , (c) w , (d) ω_z .

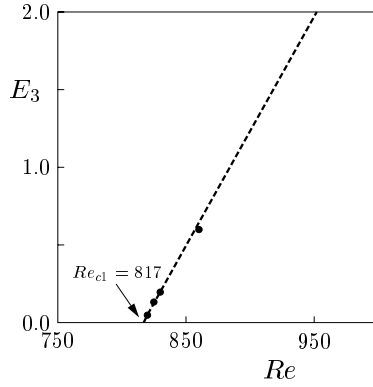


Figure 5. Kinematic energy E_3 of the Fourier mode with $k = 3$. $\Gamma = 0.6$.

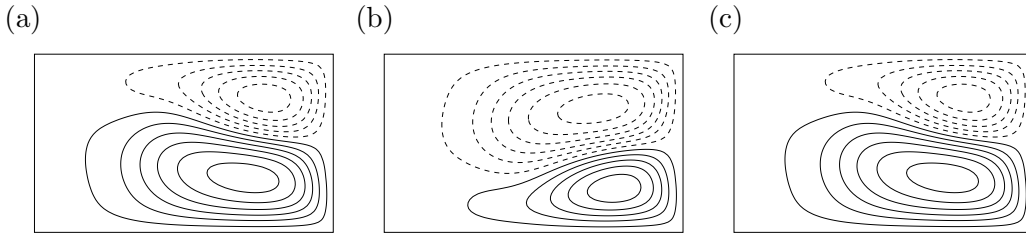


Figure 6. Flow pattern (stream lines) at different meridional planes. $\Gamma = 0.6$. $Re = 1000$. Solid line: positive value of the stream function. Dashed line: negative value of the stream function. (a) $\theta = 0$. (b) $\theta = \pi/3$. (c) $\theta = 2\pi/3$.

(Fig. 6(a)), one vortex occupies a larger portion of the section at the expense of the other. The flow pattern in the section of $\theta = \pi/3$ (Fig. 6(b)) looks like a mirror reflection of Fig. 6(a) with respect to the inter-disk midplane, and a similar flow pattern to Fig. 6(a) is observed in the section of $\theta = 2\pi/3$ (Fig. 6(c)). Thus, we can see from Fig. 6 that the spatial structure of the flow field has the shift-and-reflect symmetry with $2\pi/3$ -periodicity in the azimuthal direction, and the flow pattern oscillates periodically in each meridional plane. In order to explore the origin of the time-periodic flow, we examine the temporal behaviour of the axial velocity in the meridional plane. The axial velocity w_1 at the point $(\xi, \theta, z) = (0.8, 0, 0.5\Gamma)$ is adopted as the characteristic quantity which manifests the magnitude of the asymmetry of the flow field in a

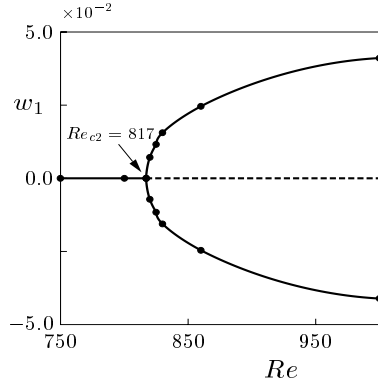


Figure 7. Bifurcation diagram. $\Gamma = 0.6$. w_1 : axial velocity at the point $(\xi, \theta, z) = (0.8, 0, 0.5\Gamma)$. Solid line: stable solution. Dashed line: unstable solution.

meridional plane. The bifurcation diagram obtained for $\Gamma = 0.6$ is shown in Fig. 7, where the minimum and maximum values of the velocity in one oscillation period are plotted against Re , and the solid and dashed lines indicate stable and unstable solutions, respectively. As shown in fig. 7, the steady symmetric flow with respect to the inter-disk midplane is stable in the range of $Re < Re_{c2} = 817$, and unstable for $Re > Re_{c2}$. A supercritical Hopf bifurcation occurs at $Re = Re_{c2}$, from which a time-periodic solution bifurcates. The critical Reynolds number obtained from this diagram is consistent with the value of Re_{c2} determined from Fig. 5, at which a steady symmetric flow loses axisymmetry. Hence, we conclude that the flow field becomes non-axisymmetric as well as asymmetric with respect to the inter-disk midplane simultaneously as the Reynolds number exceeds a critical value, and resultantly a polygonal flow pattern and oscillation are observed in the horizontal and meridional plane, respectively.

4.2. Linear stability analyses

We carried out the linear stability analysis of the basic axisymmetric flow to non-axisymmetric disturbances to explore the origin of the polygonal flow pattern. In numerical calculation of the stability analysis, the number of 100×100 mesh points was adopted. Figure 8 shows the linear growth rate of the disturbance with a wavenumber k for $\Gamma = 0.6$. The critical Reynolds number Re_c at which the basic flow loses its stability is determined by plotting the linear growth rate of each non-axisymmetric disturbance with $k = 3$ as a function of Re . We determined from this figure the critical Reynolds number and wavenumber to be $Re_c = 800$ and $k_c = 3$ respectively. The basic flow becomes unstable to the non-axisymmetric disturbance with $k = 3$ at $Re_c = 800$. This result agrees with the one obtained in numerical simulation. The flow pattern of the disturbance for $\Gamma = 0.6$ at critical Reynolds number is presented in Fig. 9. This figure shows the stream function of the disturbance at different meridional planes sectioned in every half wavelength. The stream function of the disturbance is symmetric with respect to the r -axis, whereas that of the basic flow shows the anti-symmetry as indicated in Fig. 3. The stream function of the disturbance shows the symmetry, which is opposite to that of the basic flow, and changes its sign with $\pi/3$ -periodicity in the azimuthal direction. From these results, it is shown that above the critical Reynolds number, the non-axisymmetric disturbance grows and the basic flow loses its stability. Accordingly, as shown in preceding subsection, the polygonal flow pattern appears in the horizontal plane (Fig. 4) and the flow field displays the shift-and-reflect symmetry in the meridional plane (Fig. 6).

For a smaller length ratio, $\Gamma = 0.2$, the stability of the basic flow was examined using the linear stability analysis and the flow visualization technique in experiment. The critical Reynolds

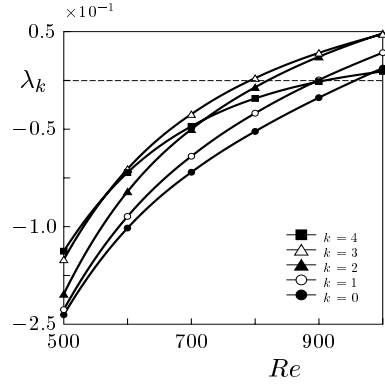


Figure 8. Linear growth rate λ_k . $\Gamma = 0.2$.

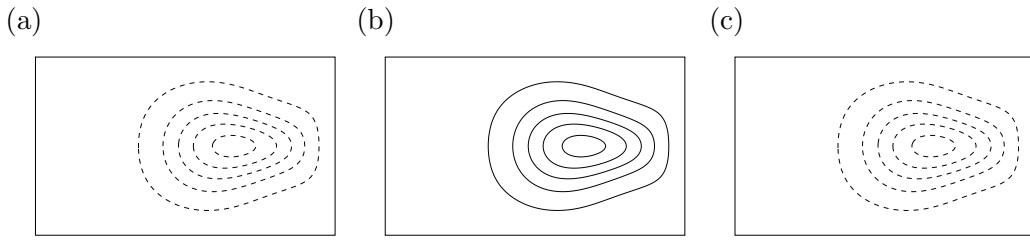


Figure 9. Flow pattern of disturbance at different meridional planes. $\Gamma = 0.6$. $Re = 800$. Solid line: positive value of the stream function. Dashed line: negative value of the stream function. (a) $\theta = 0$. (b) $\theta = \pi/3$. (c) $\theta = 2\pi/3$.

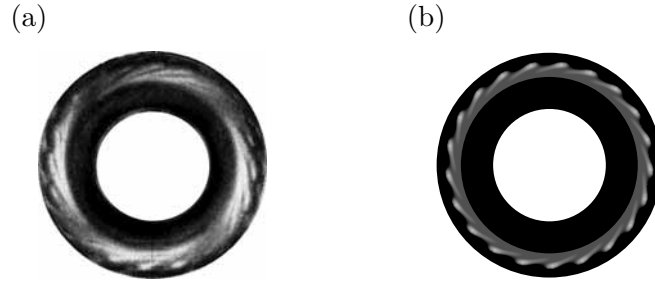


Figure 10. Flow pattern in the horizontal plane. $\Gamma = 0.2$. (a) Experimental result. $Re = 2630$. (b) Numerical result. $Re = 2660$.

number Re_c and wavenumber k_c are evaluated numerically in the same way with the case of $\Gamma = 0.6$. As a result, we determined $Re_c = 2660$ and $k_c = 21$ for $\Gamma = 0.2$. It was found that the most unstable mode of the disturbance has an unexpected wavenumber $k_c = 21$. We can see from this result that for $\Gamma = 0.2$, the basic flow first becomes unstable to a non-axisymmetric disturbance, i.e. the axisymmetry-breaking occurs as the first instability as the case of $\Gamma = 0.6$. Also, we confirm that for $\Gamma = 0.2$, the disturbance has the same spatial symmetry observed in the meridional plane for the case of $\Gamma = 0.6$. Thus, we confirmed that the first bifurcation from the basic flow is caused by the same type of instability for $\Gamma = 0.2$ as for $\Gamma = 0.6$.

Figures 10 (a) and 10 (b) compare the visualized flow field in experiment with the vorticity field obtained by numerical calculation for $\Gamma = 0.2$. The vorticity field with a wavenumber

$k = 21$ at $Re = 2660$ (Fig. 10(b)) was composed by adding the disturbance to the basic flow, where an appropriate multiplier to the disturbance is assumed by estimating the magnitude of the disturbance. As shown in Fig. 10 (a), the flow field at $Re = 2630$ obtained in experiment is composed of about twenty vortices arranged along the region of rigid-body rotation. The visualized flow pattern in experiment shows good agreement with the vorticity field obtained by numerical calculation.

References

- [1] Lennemann E 1974 *IBM J. Res. Develop.* **18** 480–488
- [2] Abrahamson S D, Eaton J K and Koga D J 1989 *Phys. Fluids A* **1** 241–251
- [3] Schuler C A, Usry W, Weber B, Humphrey J A C and Greif R 1990 *Phys. Fluids A* **2** 1760–1770
- [4] Humphrey J A C and Gor D 1993 *Phys. Fluids A* **5** 2438–2442
- [5] Humphrey J A C, Schuler C A and Webster D R 1995 *Phys. Fluids* **7** 1225–1240
- [6] Herrero J, Humphrey J A C and Giralt F 2002 *ASME J. Fluids Eng.* **124** 719–727
- [7] Herrero J, Giralt F and Humphrey J A C 1999 *Phys. Fluids* **11** 88–96
- [8] Hirata K, Furue M, Sugawara N and Funaki J 2005 *J. Phys.: Conf. Series* **14** 213–219
- [9] Randriamampianina A, Schiestel R and Wilson M 2001 *J. Fluid Mech.* **434**, 39–64